

Elevated temperature mechanical behaviour of nanoquasicrystalline $\text{Al}_{93}\text{Fe}_3\text{Cr}_2\text{Ti}_2$ alloy and composites

S. Pedrazzini ^{a,b,*}, M. Galano ^b, F. Audebert ^{b,c,d}, G.D.W. Smith ^b

a Department of Materials Science and Metallurgy, University of Cambridge, 27 Charles Babbage Road, CB3 0FS Cambridge, UK

b Department of Materials, University of Oxford, Parks Road, OX1 3PH Oxford, UK

c Advanced Materials Group, INTECIN (CONCET-UBA), Facultad de Ingeniería, Universidad de Buenos Aires, Paseo Colón 850, Buenos Aires 1063, Argentina

d Department of Mechanical Engineering and Mathematical Sciences, Oxford Brookes University, Wheatley Campus, OX33 1HX Oxford, UK

Rapidly solidified nano-quasicrystalline $\text{Al}_{93}\text{Fe}_3\text{Cr}_2\text{Ti}_2$ at% alloy has previously shown outstanding tensile and compressive strength and microstructural stability up to elevated temperatures. Despite this, no study had previously assessed the effect of plastic deformation at elevated temperature to simulate thermal-mechanical forging processes for the production of engineering components. The present work analysed bars consisting of a nano-quasicrystalline $\text{Al}_{93}\text{Fe}_3\text{Cr}_2\text{Ti}_2$ at% alloy matrix, with the addition of 10 and 20 vol% pure Al ductilising fibres, produced through gas atomisation and warm extrusion. The microstructure was made primarily of nanometre-sized icosahedral particles in an α -Al matrix. Compression tests were performed across a range of temperatures and strain rates. The measured yield strength at 350 °C was over 3x that of “high strength” 7075 T6 Al alloy, showing outstanding thermal stability and mechanical performance. However, the microstructure was shown by XRD to undergo a phase transformation which resulted in the decomposition of the icosahedral phase around ~500 °C into more stable intermetallic phases. Serrated flow associated with dynamic strain ageing was observed and a semi-quantitative analysis matching elemental diffusion speeds with dislocation speed at specific strain rates was performed, which tentatively identified Ti as the solute species responsible within the selected range of temperatures and strain rates.

1. Introduction

Recent developments in novel high-performance aluminium based alloy systems strengthened with nano-scale dispersoid phases have made them very attractive lightweight materials to be used in engineering components. Rapidly solidified $\text{Al}_{93}\text{Fe}_3\text{Cr}_2\text{Ti}_2$ alloy, made of sub-micron sized icosahedral quasicrystalline phases in an α -Al matrix, has been studied because of its improved strength at elevated temperatures compared to current commercially available Al alloys [1,2]. The applications of this alloy have however previously been limited by temperature sensitivity, reduced ductility and response to bulk processing routes. Currently, for any application above ~200 °C Ti alloys are used despite the fact that they are heavier, overdesigned and more expensive for use in applications below ~300–350 °C [1]. Nano-quasicrystalline Al-Fe-Cr-Ti based alloys have shown a reduced plastic regime during mechanical testing and therefore reduced energy absorption ability in quasi-static tests at room temperature compared to commercial 7xxx and 2xxx series Al alloys [1,3–5]. In an effort to improve the ductility Nagy et al. showed that creating

composites using nano-quasicrystalline Al-Cu-Fe and Al-V-Fe alloy matrices with pure Al fibres gave improved strain-to-failure in room temperature tensile tests [6]. In the present work, 10% and 20% volume fractions of pure Al fibres have been added to a nano-quasicrystalline $\text{Al}_{93}\text{Fe}_3\text{Cr}_2\text{Ti}_2$ at% alloy matrix in an effort to improve ductility in mechanical tests at varying strain rates [7]. Some studies have been found in the literature on the thermal stability of this alloy [8,9] and a few on high temperature mechanical testing [1,2], however, no studies were found that analyse the alterations to the strength and microstructure brought by industrially used processing methods which involve thermal mechanical forging, the knowledge of which is essential towards safe use in engineering applications. Dynamic strain ageing (DSA) is a common occurrence in Al-based alloys, and can be observed in the form of serrated tensile stress-strain curves [10]. DSA has been shown to reduce the ductility of the material at higher temperature, and to reverse the strain rate effects on the ultimate tensile strength (UTS) of the alloys [10]. Serrated flow in tensile stress strain curves is extremely common in a very broad range of commercial and non-commercial Al-based alloys where substitutional or interstitial solutes have been considered responsible [11]. This phenomenon can be observed at room temperature only in alloys which have smaller mobile solute atoms like Si or Li that can “pin” dislocations by diffusing faster than the dislocations move and placing themselves directly underneath the extra half plane in a very stable low energy position [11]. A higher amount of energy is then required in order to move the dislocation, which can then be pinned again by the fast diffusion of the solute atoms. This gives rise to serrated flow in tensile stress-strain curves. At high temperatures the DSA effect is observed in substitutional alloy systems and the solutes to which this effect is attributed generally include Mg, Cu and Mn [11] but high temperature deformation has suggested the probability of Fe as a solute also responsible for serrated flow [11]. Skinner et al. [12] used an Al-SiX alloy with X being a transition element, such as Ti or Fe and proved that at room temperature DSA behaviour was caused by the migration of the Si atoms interfering with dislocation motion, but over $\sim 167^\circ\text{C}$ the titanium atoms also started contributing to this effect and the Fe atoms started contributing too at temperatures above $\sim 227^\circ\text{C}$. All the alloys in Skinner's study showed ductility reductions at temperature ranges that varied depending on which solute atom was in solid solution and depending on the strain rate of the tests. DSA does not require high concentrations of solute atoms to occur. It has been shown that impurity atoms alone may result in serrated flow in commercially pure Al [11], however the effect is more evident with increasing solute concentrations [12]. The present work investigates materials processing conditions for commonly used industrial practices such as forging and hot rolling, through a series of compression tests at varying strain rates and temperatures. These tests were also used to investigate dynamic strain ageing behaviour through a semi-quantitative analysis to determine which species in solid solution (Fe, Cr or Ti) was likely to cause the serrations.

2. Experimental procedure

Compression tests specimens were prepared from the extruded bars using a lathe, and were cylinders 15 mm in length and 10 mm in diameter. Details of the extrusion conditions, production and microstructural characterisation can be found in a previously published study [7]. Extra care was taken in order to ensure the sides were flat and polished with 1200 grit SiC paper for even induction heating during tests. A thermocouple was welded to the centre of each specimen before it was induction heated to the selected temperature and compressed using a Gleeble 3500 machine between WC discs. No sheets or paste was added between the sample and the WC discs. True stress-true strain values were calculated assuming conservation of volume. Barrelling was found to be minimal, due to the brittle nature of the samples and was therefore neglected in the true stress-true strain calculations. The selected temperatures were 350°C , 400°C , 450°C and 500°C at strain rates 0.1, 1, 10 and 50 s^{-1} . These temperatures and strain rates were selected to

analyse the feasibility of forging the alloy and composites into engineering components. The compression test samples were then polished and analysed by XRD to detect phase transformations occurring during testing. A Philips 1810 θ - 2θ diffractometer was used. The scanning angles 2θ used were 20–100°, voltage of 35 kV, current of 50 mA and step size 0.02°. A combination of data sheets [13] and published papers [14,15] was used for indexation of the peaks. DSC was performed in order to identify the temperature range in which phase transformations occurred and followed by transmission electron microscopy coupled with energy dispersive X-ray spectroscopy (TEM-EDX) identification of the phases present in the alloy. A Philips CM20 TEM was used with Oxford Instruments EDX detector and data was then analysed using INCA software.

3. Results

Fig. 1 shows true stress-true strain curves from the compressive tests of the monolithic $\text{Al}_{93}\text{Fe}_3\text{Cr}_2\text{Ti}_2$ bar plotted with a constant initial strain rate and varying temperature between 350–500 °C. The curves displayed in Fig. 1(a), (b), (c) and (d) show that at constant strain rate the yield strength decreases with increasing temperature. Also, the gradient of the plastic zones of all the curves at constant strain rate varies with changing temperature. A negative gradient of the plastic zone of the compressive true stress-true strain curve indicates that the material is softening under the applied stress, a positive gradient indicates that the material is hardening. If the gradient is zero, that indicates a steady state. Fig. 1(a) shows three curves, all taken at strain rate 0.1 s^{-1} . The curve at $T = 500 \text{ °C}$ is hardening (with the gradient being 12% higher than the steady-state value), the curve at $T = 450 \text{ °C}$ is at a steady state (gradient = 0) and the one at $T = 350 \text{ °C}$ is softening. Serrated flow can be observed at 350 °C and 450 °C at strain rates 0.1 s^{-1} and at 350 °C at strain rate 1 s^{-1} in the curves in Fig. 1(a) and (b). All the three curves measured at strain rate 1 s^{-1} and shown in Fig. 1(b) show a softening behaviour, more evident with a steeper gradient at 350 °C, in the early stage of plastic deformation however they flatten into a steady state between true strain 0.6–0.8. In Fig. 1(c) the three curves at strain rate 10 s^{-1} are shown. All three curves also show a softening behaviour in the plastic zone, with the lowest temperature curve showing the steepest decreasing slope. All three curves also have a shallower gradient between true strains 0.6–0.8. Fig. 1(d) shows the two curves taken at the highest strain rate: 50 s^{-1} . Multiple large steps can be observed at the onset of plastic deformation in both curves obtained at strain rate 50 s^{-1} with more of a softening effect in the lower temperature curve at 400 °C. Large steps could be associated with increasing uncertainty in the Gleeble measurements at higher strain rates. X-ray diffraction studies have been performed on the samples and are shown in Fig. 2. They show the thermal evolution of the samples after compression testing at different temperatures between 350–500 °C. The icosahedral phase was labelled “i”, the FCC-Al matrix was labelled α , then ϕ was $\text{Al}_{13}\text{Cr}_2$, ζ was $\text{Al}_{13}\text{Fe}_4$ and κ was Al_3Ti . XRD peaks were indexed as follows. α -Al peaks were identified by indexing the reflections corresponding to the (111), (200), (220), (311), (222) and (400) planes in the $2\theta = 10^\circ$ – 100° range at 38.5° (100% intensity), 44.7° , 65.2° , 78.3° , 82.5° and 99.2° [13]. The presence of the icosahedral phase was shown by broad peaks at $2\theta \sim 22.9^\circ$, 41.3° , 43.5° , 61.6° and 73.7° [14]. Other intermetallic phases were identified including Al_3Ti , $\text{Al}_{13}\text{Fe}_4$, $\text{Al}_{13}\text{Cr}_2$ which were indexed using data sheets [13]. The presence of Al_3Ti was shown by the peaks at $2\theta \sim 22.3^\circ$, 31.9° , 39.2° (100% intensity), 66.5° and 84.4° corresponding to the (100), (110), (111), (220), (311) reflections respectively. The $\text{Al}_{13}\text{Fe}_4$ was shown by peaks at 43.1° , 44.2° and 44.4° corresponding to the 100% intensity (623) reflection and the (025) and (423) respectively. The $\text{Al}_{13}\text{Cr}_2$ phase was shown by the peaks at 36.6° , 41.2° , 41.4° , 41.5° , 43.8° , 43.9° (100% intensity),

44.0°, 75.3°, 75.7° corresponding to the (131), (1113), (711), (424), (1022), (820), (333), (15 3 7) and (335). After testing at 350 °C, four phases could be identified by XRD: α -Al, icosahedral quasicrystals, $\text{Al}_{13}\text{Fe}_4$ and $\text{Al}_{13}\text{Cr}_2$. As the temperature increased, the peaks arising from $\text{Al}_{13}\text{Fe}_4$ and $\text{Al}_{13}\text{Cr}_2$ phases became more pronounced, while the peaks corresponding to the icosahedral phase decreased. At 500 °C, the icosahedral phase could not be indexed by XRD, indicating its complete dissolution. Al_3Ti was also detected at 500 °C. According to other authors at ~500 °C the decomposition of the icosahedral phase occurs, producing more stable intermetallic phases [9]. This observation was confirmed using a DSC to detect the exact range of temperatures in which the phase transformation occurred and a TEM to characterise the microstructure before and after exposure to 500 °C. The DSC curve is shown in Fig. 3, and it shows a single-phase transformation occurring in the range of 400–500 °C. TEM characterisation of the samples after heating to 500 °C was also performed. The micrographs are shown in Fig. 4 along with some EDX compositional analysis of some of the phases shown in Table 1. The characterisation of the samples before mechanical testing was also performed, and has been published as part of a previous paper [16].

Elongated, nodular phases which can be seen in Fig. 4(a) and at higher magnification in Fig. 4(b) were shown by EDX to be Fe-enriched and therefore $\text{Al}_{13}\text{Fe}_4$, although overlap with the matrix and other phases made the chemical composition difficult to measure individually. Fig. 5 shows the true stress-true strain curves at constant strain rates of the 10 vol% fibre composite. From the curves presented in Fig. 5(b), (c), (d) and (e) we can see that an increase in temperature causes a decrease in the yield strength. It is also noticeable that the gradient of the plastic zones of all the curves at constant strain rate varies with changing temperature. Fig. 5(b) shows the curves taken at strain rate 0.1 s^{-1} . The curves at $T = 500 \text{ °C}$ and $T = 450 \text{ °C}$ are both hardening, the curve at $T = 400 \text{ °C}$ is at a steady state and the one at $T = 350 \text{ °C}$ is softening. All four curves taken at strain rate 1 s^{-1} at $T = 350 \text{ °C}$, 400 °C , 450 °C and 500 °C and shown in Fig. 5(c) show a softening behaviour in the plastic zone, more evident with a steeper gradient at 350 °C . They show softening in the early stage of plastic deformation however they reach a steady state between true strain 0.6–0.8. In Fig. 5(d) the four curves at strain rate 10 s^{-1} are shown. All of the curves show a softening behaviour in the plastic zone, with the lowest temperature curve showing the steepest decreasing slope. They also have a flatter gradient between true strains 0.6–0.8. Fig. 5(e) shows the four curves taken at 50 s^{-1} strain rate. The effect of the fibre addition has been studied by also plotting the tests performed on the bar with 20 vol% fibres in Fig. 6 and using them for comparison. A temperature increase causes a decrease in yield strength of the samples. From the curves presented in Fig. 6(a), (b), (c) and (d), it can also be observed that the gradient of the plastic zones of all the curves at constant strain rate varies with changing temperature. Fig. 6(a) shows the curves taken at strain rate 0.1 s^{-1} . The curve at $T = 500 \text{ °C}$ is hardening, the curve at $T = 450 \text{ °C}$ is at a steady state and the ones at $T = 400 \text{ °C}$ and $T = 350 \text{ °C}$ are softening. All four curves taken at strain rate 1 s^{-1} at $T = 350 \text{ °C}$, 400 °C , 450 °C and 500 °C and shown in Fig. 6(b) show a softening behaviour in the plastic zone, more evident with a steeper gradient at 350 °C . They show softening in the early stage of plastic deformation however they flatten into a steady state between true strain 0.6–0.8. In Fig. 6(c) the four curves at strain rate 10 s^{-1} are shown. All of the curves show a softening behaviour in the plastic zone, with the lowest temperature curve showing the steepest decreasing slope. They also have a shallower gradient between true strains 0.6–0.8. Fig. 6(d) shows the four curves taken at 50 s^{-1} strain rate.

4. Discussion

4.1. Strain rate effect

The yield strength of all the samples tested is lower at lower strain rates and it increases with increasing strain rates. The measured value of yield strength of the monolithic alloy sample at 0.1 s⁻¹ strain rate was 340 MPa at 350 °C and 100 MPa at 500 °C. A value of yield strength was found in the literature for 7075 T6 Al under the same testing conditions, with the same sample size and equipment and it was 110 MPa at 350 °C, just under 1/3 of the strength of the Al₉₃Fe₃Cr₂Ti₂ alloy, decreasing to 75 MPa at 500 °C [17]. Increasing the strain rate causes a softening effect, which is evident from the slope of the curves in the plastic regime becoming steeper at higher strain rates. In the literature, several models have been proposed to describe the hot compressive behaviour of Al alloys. The traditional method considers the flow stress to have a power law dependence on the imposed strain rate [18–20]:

$$\sigma = C\dot{\epsilon}^m$$

where C is a parameter which depends on factors including the structure of the material and testing temperature and m is the strain rate sensitivity parameter, making this equation only valid at constant temperature. The strain rate sensitivity parameter quantifies the effect of strain rate on the flow stress and can be derived by finding the gradient of the plot of ln(σ) and ln($\dot{\epsilon}$) at steady state and constant temperature [21,22]. This plot can be seen in Fig. 7(a) for the monolithic alloy bar, (b) for the composite with 10 vol% fibres and (c) 20 vol % fibres. The relationship between stress and strain rate indicates that the material hardens with increasing strain rate. The strain rate sensitivity parameter can be estimated from the gradient of the curve in Fig. 7 [21]. The values of m obtained in the present study were in the range of 0.05–0.14. For comparison, the values of m measured in a 2024 alloy at 0.6–0.8 of its homologous temperature were also found to be in the range of 0.05–0.15 [22,23]. The homologous temperature is calculated by dividing the testing temperature by the melting temperature of the alloy in Kelvin. The variation of strain rate sensitivity parameter with temperature compared to the values of 2024 Al alloy [22] can be seen in Fig. 8.

4.2. Temperature effect

The effect of working temperature on the flow stress behaviour of the alloy and composites can be described by the Arrhenius-type equation [20,24,25]:

$$\dot{\epsilon} = A\sigma^n e^{\frac{-Q}{RT}}$$

where A is a constant, n is the stress exponent ($= 1/m$), R is the gas constant and Q the activation energy. At a given strain rate therefore the slope of ln(σ) and 1/T will give the value of the activation energy Q divided by m and the gas constant R (only valid in the steady state condition). This plot can be found in Fig. 9. From Fig. 9(a), (b) and (c) it is clear that the plot of ln(steady state stress) and 1/T is not perfectly linear, and that the linearity is lost particularly at the higher temperature end of the plot. This can be explained as the material undergoes a phase transformation in that temperature range. The transformation involves the decomposition of the icosahedral phase into more stable intermetallic phases. At 350 °C the microstructure was shown by XRD in Fig. 2 to consist of icosahedral phase, Al₁₃Fe₄, Al₁₃Cr₂ and FCC-Al. Between 400 and 450 °C a transition occurs, which involves the icosahedral peaks becoming less defined and the peaks of other intermetallic phases becoming sharper. The icosahedral phase could not be indexed by XRD after testing at 500 °C. The apparent activation energy can be derived from the Arrhenius plot in Fig. 9 only if the correlation is linear, which is not the present case.

4.3. Dynamic strain ageing

Dynamic strain ageing is evident in the high temperature compression tests at strain rate 0.1 s^{-1} at all the temperatures tested, between 350–500 °C, presented in Fig. 1. It is greatly reduced at strain rate 1 s^{-1} and no longer present at strain rates above that. Dynamic strain ageing causes serrations in the plastic region of the stress-strain curves. It is extremely common in a very broad range of commercial and non-commercial Al based alloys and substitutional or interstitial solutes have been considered responsible [10]. It is generally not possible to derive reliable values for the activation energies associated with DSA experimentally. In this case, it is also impossible to measure the hardening contribution to the flow stress due to DSA as the behaviour of the material without DSA is unknown. What follows is a semi-quantitative analysis which attempts to identify the species in solid solution responsible for dynamic strain ageing. The model used relies on the assumptions that a single solute species migrates without forming complexes and that the microstructure does not evolve with temperature at 350 °C. Due to the composition of this alloy, it is likely that any one or any combination of Fe, Cr or Ti found in excess of the solid solubility due to the rapid solidification production technique is responsible for dynamic strain ageing. Previously, Skinner et al. [12] used an Al-Si-Fe and Al-Si-Ti alloy and proved that at room temperature DSA behaviour was caused by the migration of the Si atoms interfering with dislocation motion, but over $\sim 167 \text{ °C}$ the titanium atoms also started contributing to this effect and over 227 °C the Fe atoms started contributing too. All their alloys in this study showed ductility reductions at temperature ranges that varied depending on which solute atom is in solid solution and depending on the strain rate of the tests. Bouchaud et al. worked on a rapidly solidified Al-Fe-V-Si alloy and concluded similarly that at room temperature Si atoms were responsible for this effect, but between 127 and 227 °C Fe atoms became primarily responsible for dynamic strain ageing [26]. Both the papers by Skinner et al. [12] and Bouchaud et al. [26] perform semi-quantitative analyses which rely on calculations of diffusion coefficients of substitutional atoms at different temperatures and match their speed to the speed of dislocations moving at the applied strain rate to determine which of the alloying elements is responsible for dynamic strain ageing at which temperature range. This relies on extensive testing at a variety of temperatures and strain rates to find out the minimum in ductility and the range in which it happens. In the current study tests were performed at strain rates $0.1\text{--}50 \text{ s}^{-1}$ and temperatures between 350–500 °C. Previous compression tests performed on the same alloy composition both at room temperature and 250 °C and a strain rate $1 \times 10^{-4} \text{ s}^{-1}$ did not show serrated flow [27], so the range in which serrated flow is visible can be narrowed down to between 250–400 °C and 1×10^{-4} and 1 s^{-1} strain rates. Based on the current set of data, the starting point cannot be established more precisely, therefore temperature values from the literature will be used to perform a semi-quantitative analysis which estimates the diffusion coefficients in an attempt to tentatively identify which species is likely to cause DSA at the selected testing temperature of 350 °C (625 K). Diffusion coefficients can be calculated at the strain rate and temperature which correspond to the strain rate sensitivity minimum using the formula used by Bouchaud et al. [26]:

$$D = \left(\frac{k_B T}{3|W|} \right) \left(\frac{b^2}{\tau} \right) \left(\frac{c_1}{\pi c_0} \right)^{3/2}$$

Where k_B is the Boltzmann constant 1.38×10^{-23} , T is the temperature at which SRS effect is minimum, W is the absolute value of the interaction energy between dislocations and diffusing species, b is the Burgers vector (for pure Al = 0.286 nm [26]), c_1 is the concentration of solute atoms at dislocation line at saturation (typically 0.5), c_0 is the total concentration of diffusing

species (total number of diffusing atoms/total number of atoms) and τ is the relaxation time [26]. Solutes in solid solution would be expected to decrease when the rapidly solidified alloy is kept elevated temperatures, but as the compression tests were induction heated for less than 5 min to reach and stabilise the required temperature, therefore these calculations have been performed using the values of solutes in solid solution before heat treatment. The values, previously quoted in the authors work [7] were $\text{Al}_{\text{bal}}\text{Fe}0.2\pm0.1\text{Cr}0.4\pm0.2\text{Ti}1.3\pm0.2$ as measured by TEM-EDX over 10 measurements. When ductility and strain rate sensitivity are minimum Orowan's law says that [26]:

$$\tau = t_w = (b\rho_m\rho_f^{-\frac{1}{2}})/\dot{\epsilon}$$

Where ρ_m is the density of mobile dislocations (in rapidly solidified extruded Al-Fe-V-Si $\sim 10^{11} \text{ m}^{-2}$ [26]), ρ_f is the density of forest obstacles ($\sim 10^{12} \text{ m}^{-2}$ [26]), $\rho_f^{-1/2}$ is the mean spacing between forest obstacles, b is the burgers vector, $\dot{\epsilon}$ is the strain rate, in this case 0.1 s^{-1} . Matching the diffusion coefficient equation with the dislocation speed at the ductility minimum, the equation to calculate diffusion coefficients becomes [26]

$$D = \left(\frac{kT}{3|W|} \right) \left(\frac{b\dot{\epsilon}}{\rho_m\rho_f^{-\frac{1}{2}}} \right) \left(\frac{c_1}{\pi c_0} \right)^{3/2}$$

The interaction energy between dislocations and diffusing species W can be calculated as follows: the interaction energy varies from 0 to W_{\min} when the impurity atom reaches a dislocation. A measure of the limiting values of concentration (c_0) and temperature (T) at which dynamic strain ageing can occur is given by

$$c_0 \geq c_1 \exp\left(\frac{W}{kT}\right) \quad [28,29].$$

W is at a minimum when impurity atom reaches a dislocation $\text{soc}_0 = c_1 \exp\left(\frac{W_{\min}}{kT}\right) \quad [28,29]$

When the force between the dislocation and the impurity atom is attractive, $c_1 \sim 0.5$ [29] so

$$W_{\min} = kT \ln \left(\frac{c_0}{0.5} \right)$$

Applying this formula to the current experimental values and using temperatures taken from the literature for the point of minimum ductility caused by Ti and Fe atoms in solid solution, the diffusion coefficients obtained are of the order of $\sim 10^{-16}$ for Fe, 10^{-16} for Cr and $\sim 10^{-18}$ for Ti, as seen in Table 2. As a comparison, values taken from the literature of tracer impurity diffusion coefficients of Ti in Al at 625 K are in the order of magnitude of $10^{-17} \text{ m}^2/\text{s}$, for Fe in Al $10^{-18} \text{ m}^2/\text{s}$ [30]. The diffusion coefficient is however influenced also by both the mechanical deformation at the applied strain rate and the concentrations, which values from the literature do not account for. Therefore the diffusion coefficients calculated in Table 2 are more accurate than the literature values given for comparison. It is generally accepted in literature that DSA occurs when the diffusion coefficient is of the order of $D \sim 10^{-18} \text{ m}^2/\text{s}$ [26,29]. The semiquantitative analysis whose results are available in Table 2 would tentatively suggest that Ti could be a likely solute to cause DSA at the selected temperature at which the compression tests were made of 625 K. Robinson and Shaw say evidence suggests that the T_{\min} occurs at $T \sim 0.3T_m$ where T_m is the homologous

melting temperature. Assuming T_m is ~ 660 °C, then $T_{min} \sim 198$ °C, which is also close to the values taken from Bouchaud and Skinnners papers [11,12,26].

5. Conclusions

1. The compressive strength of the nanoquasicrystalline $Al_{93}Fe_3Cr_2Ti_2$ alloy at 350 °C was between 2-3x that of “high strength” 7075 T6 alloy tested under the same conditions.
2. The effect of strain rate variations was explained using a power law creep model with strain rate sensitivity coefficient which decreased linearly between the values of $m = 0.05$ - 0.14 with increasing temperature.
3. Between 350 and 500 °C the icosahedral phase underwent a phase transformation which resulted in its decomposition into more stable intermetallic phases.
4. The high temperature compressive data at strain rates between 0.1 and 50 s^{-1} and temperatures between 350–500 °C, used for the first time in a semi-quantitative analysis to determine which species in solid solution (Fe, Cr or Ti) was likely to cause serrated flow, suggested the Ti in solid solution in the matrix could be the most likely candidate under those conditions.

Acknowledgements

The authors would like to thank ALPOCO Ltd. and more specifically Steve McArthur who provided the powders. Asuncion Garcia Escorial and Marcela Lieblich from CENIM, Madrid extruded the powders into bars. Compression tests were performed by Bruno Hubig thanks to a collaboration with Ramiro Mazzina from Tenaris (TechInt Group), Buenos Aires, Argentina. S. Pedrazzini would like to thank Enrique Galindo-Nava from the University of Cambridge for helpful discussions. M. Galano thanks RAEng and EPSRC for their financial support through EP/G05794X/1. F. Audebert thanks UBACyT 20020130100663 and PIDDEF 31/14 for financial support.

References

- [1] A. Inoue, H. Kimura, High-strength aluminium alloys containing nanoquasicrystalline particles, *Mater. Sci. Eng. A286* (2000) 1–10.
- [2] M. Galano, F. Audebert, I.C. Stone, B. Cantor, Nanoquasicrystalline Al-Fe-Cr-based alloys Part II: mechanical properties, *Acta Mater.* 57 (2009) 5120–5130.
- [3] F. Audebert, et al., Structural characterisation and mechanical properties of nanocomposite Al-based alloys, *Mater. Trans. A* 43 (8) (2002) 2017.
- [4] A. Inoue, Amorphous, nanoquasicrystalline and nanocrystalline alloys in Al-based systems, *Prog. Mater. Sci.* 43 (5) (1998) 365–520.
- [5] W. Bolton, *Engineering Materials Technology*, Newnes, 1993.
- [6] J. Nagy, M. Balog, K. Ibdinskc, F. Simandek, P. Švec, D. Janidkovid, High strength potential of aluminium nanocomposites reinforced with nonperiodical phases, *Int. J. Mater. Prod. Technol.* 23 (1–2) (2005) 79–90.
- [7] S. Pedrazzini, et al., Strengthening mechanisms in an Al-Fe-Cr-Ti nano-quasicrystalline alloy and composites, *Mater. Sci. Eng. A* 672 (2016).
- [8] M. Galano, F. Audebert, B. Cantor, I. Stone, Structural characterisation and stability of new nanoquasicrystalline Al-based alloys, *Mater. Sci. Eng. A* 375–377 (2004) 1206–1211.

- [9] I. Todd, Z. Chlup, J.G. O'Dwyer, M. Liebllich, A. Garcia-Escorial, The influence of processing variables on the structure and mechanical properties of nano-quasicrystalline reinforced aluminium alloys, *Mater. Sci. Eng. A* 375–377 (2004) 1235–1238.
- [10] J.M. Robinson, Serrated flow in Al—base alloys, *Int. Mater. Rev.* 39 (1994) 217–227.
- [11] J.M. Robinson, M.P. Shaw, Microstructural and mechanical influences on dynamic strain aging phenomena, *Int. Mater. Rev.* 39 (3) (1994) 113.
- [12] D. Skinner, S. Zedalis, P. Gilman, Effect of strain rate on tensile ductility for a series of dispersion strengthened aluminum-based alloys, *Mater. Sci. Eng. A* 119 (1989) 81–86.
- [13] JCPDS, International Centre for Diffraction Data v2.02. p. Codes: 04-0787, 13-0146, 29-0014, 29-0042, 1999.
- [14] M. Galano, F. Audebert, I.C. Stone, B. Cantor, Nanoquasicrystalline Al-Fe-Cr-based alloys: Part I: phase transformations, *Acta Mater.* 57 (2009) 5107–5119.
- [15] F. Audebert, R. Colaco, R. Vilar, H. Sirkin, Laser cladding of Al-based quasicrystalline alloys, *Scr. Mater.* 40 (1999) 551–554.
- [16] S. Pedrazzini, et al., Strengthening mechanisms in an Al-Fe-Cr-Ti nano-quasicrystalline alloy and composites, *Mater. Sci. Eng. A* 672 (2016).
- [17] Y.C. Lin, L.T. Li, Y.X. Fu, Y.Q. Jiang, Hot compressive deformation behavior of 7075 Al alloy under elevated temperature, *J. Mater. Sci.* 47 (3) (2012) 1306–1318.
- [18] S.V.S.N. Murty, B.N. Rao, B.P. Kashyap, On the hot working characteristics of 6061Al–SiC and 6061–Al₂O₃ particulate reinforced metal matrix composites, *Compos. Sci. Technol.* 63 (1) (2003) 119–135.
- [19] Y. Frank, Su, Y. Chen, C. Tsao, Workability of spray-formed 7075 Al alloy reinforced with SiCp at elevated temperatures, *Mater. Sci. Eng. A* 364 (2004) 296–304.
- [20] V. Srivastava, V. Jindal, V. Uhlenwinkel, K. Bauckhage, Hot-deformation behaviour of spray-formed 2014 Al + SiCp metal matrix composites, *Mater. Sci. Eng. A* 477 (2008) 86–95.
- [21] D. Sastry, Y.V.R. Prasad, S. Deevi, Influence of temperature and strain rate on the flow stress of an FeAl alloy, *Mater. Sci. Eng. A* 299 (1–2) (2001) 157–163.
- [22] W.F. Hosford, R.M. Caddell, *Metal Forming: Mechanics and Metallurgy*, Cambridge University Press, 2011.
- [23] D.S. Fields, W.A. Backofen, Temperature and rate dependence of strain hardening in aluminium alloy 2024-0, *Trans. ASM* 51 (1959) 946.
- [24] P. Cavaliere, E. Cerri, E. Evangelista, Isothermal forging modelling of 2618 + 20% Al₂O₃p metal matrix composite, *Compos. Part A-Appl. Sci.* 35 (6) (2004) 117–122.
- [25] G. Ganesan, K. Raghukandan, R. Karthikeyan, B. Pai, Development of processing maps for 6061 Al/15% SiCp composite material, *Mater. Sci. Eng. A* 369 (1–2) (2004) 230–235.
- [26] E. Bouchaud, L. Kubin, H. Octor, Ductility and dynamic strain aging in rapidly solidified aluminum alloys, *Metall. Trans. A* 22 (5) (1991) 1021–1028.

[27] S. Pedrazzini, Characterisation and Mechanical Properties of Nanoquasicrystalline Al-based Composites for High Temperature Applications, PhD thesis, Department of Materials, University of Oxford, 2014.

[28] A. Cottrell, Dislocations and Plastic Flow in Metals, Oxford University Press, 1958.

[29] J. (Jacques) Friedel, Dislocations, Pergamon Press, 1964 (U.S.A. ed. distributed by Addison-Wesley Pub. Co., Reading, Mass.). [30] E.A. Brandes, G.B. Brooks, Smithells Metals Reference Book, ButterworthHeinemann, 1983

Figures

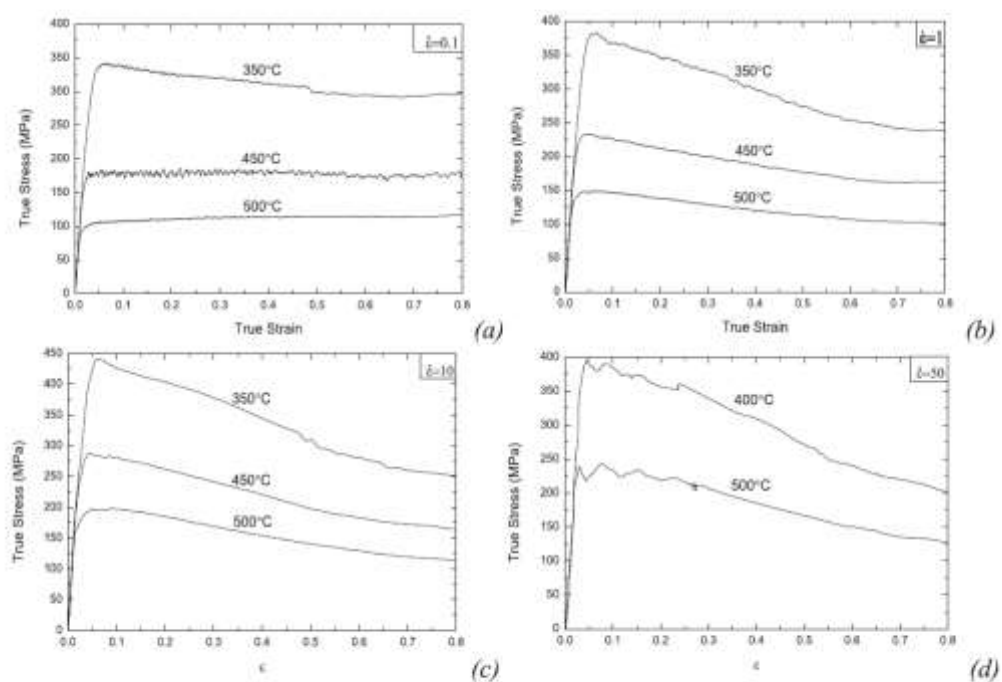


Fig. 1. Compressive tests of the monolithic alloy bar at constant strain rate and varying temperature. (a) samples tested at strain rate 0.1 s⁻¹ at temperatures 350 °C, 450 °C and 500 °C. (b) tests performed at strain rate 1 s⁻¹ and temperatures 350 °C, 450 °C and 500 °C, (c) samples tested at strain rate 10 s⁻¹ and temperatures 350 °C, 450 °C and 500 °C, (d) samples tested at strain rate 50 s⁻¹. Due to a shortage of material these could only be performed at 400 °C and 500 °C.

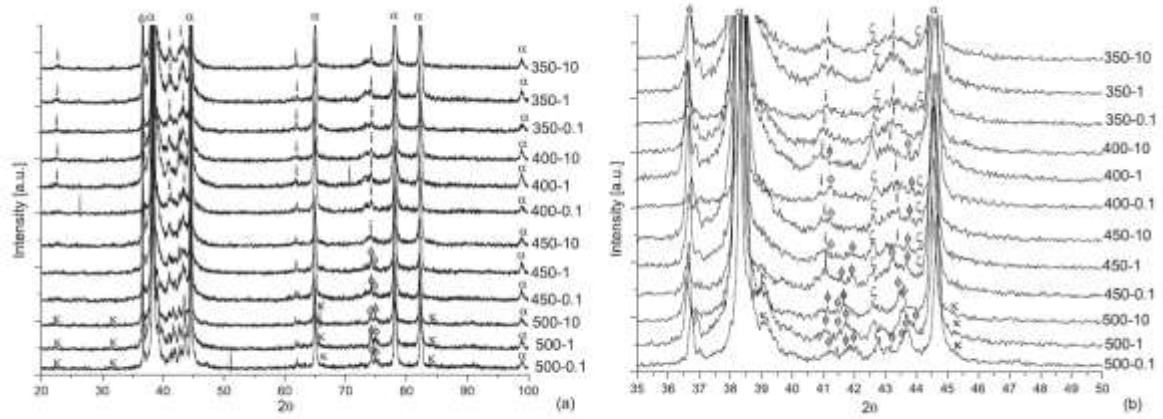


Fig. 2. X-ray diffractograms of the samples after compression testing at different temperatures and strain rates. (a) full scan from 20 to 100°, (b) enlargement of the 35–50 ° section. The curve labels represent “testing temperature – strain rate” eg. “350-10” is a sample tested at 350 °C and strain rate 10 s⁻¹.

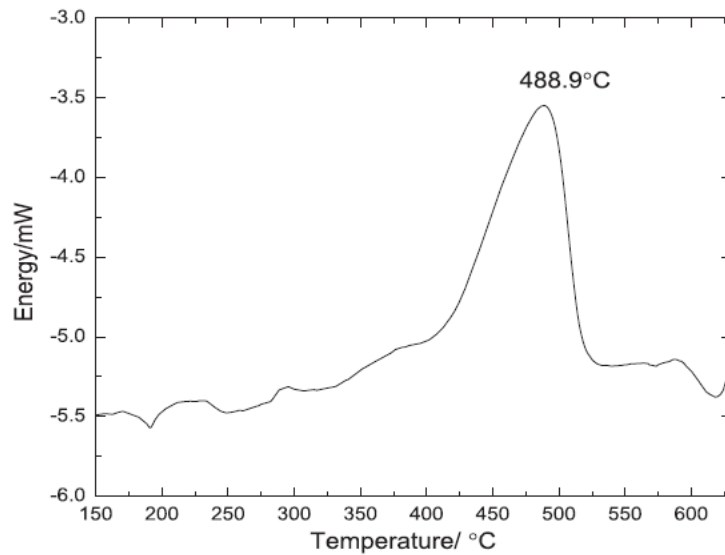


Fig. 3. DSC scan of the monolithic alloy bar performed at 40 °C/min, showing the main exothermic event occurring between 400–500 °C.

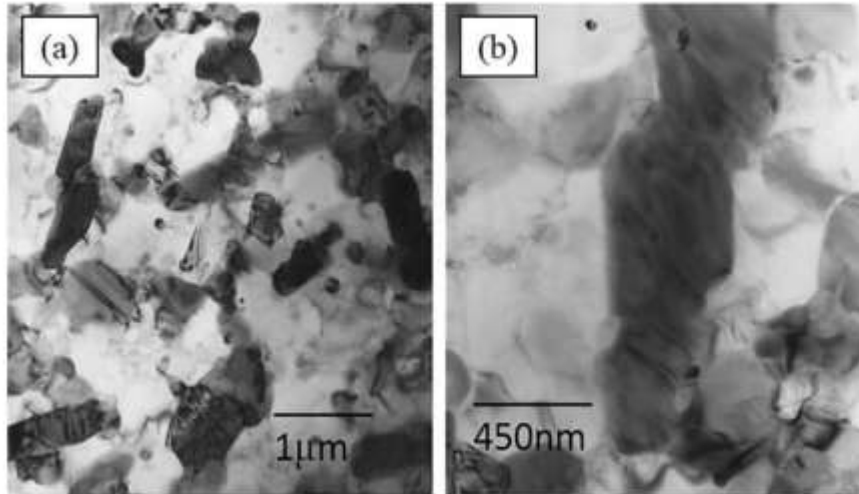


Fig. 4. Bright field TEM micrographs of the heat treated O-1a bar. (a) overview of the microstructure, (b) elongated, nodular Febased intermetallic phase. The chemical composition of the Feenriched phases in (b) measured by EDX is in Table 1.

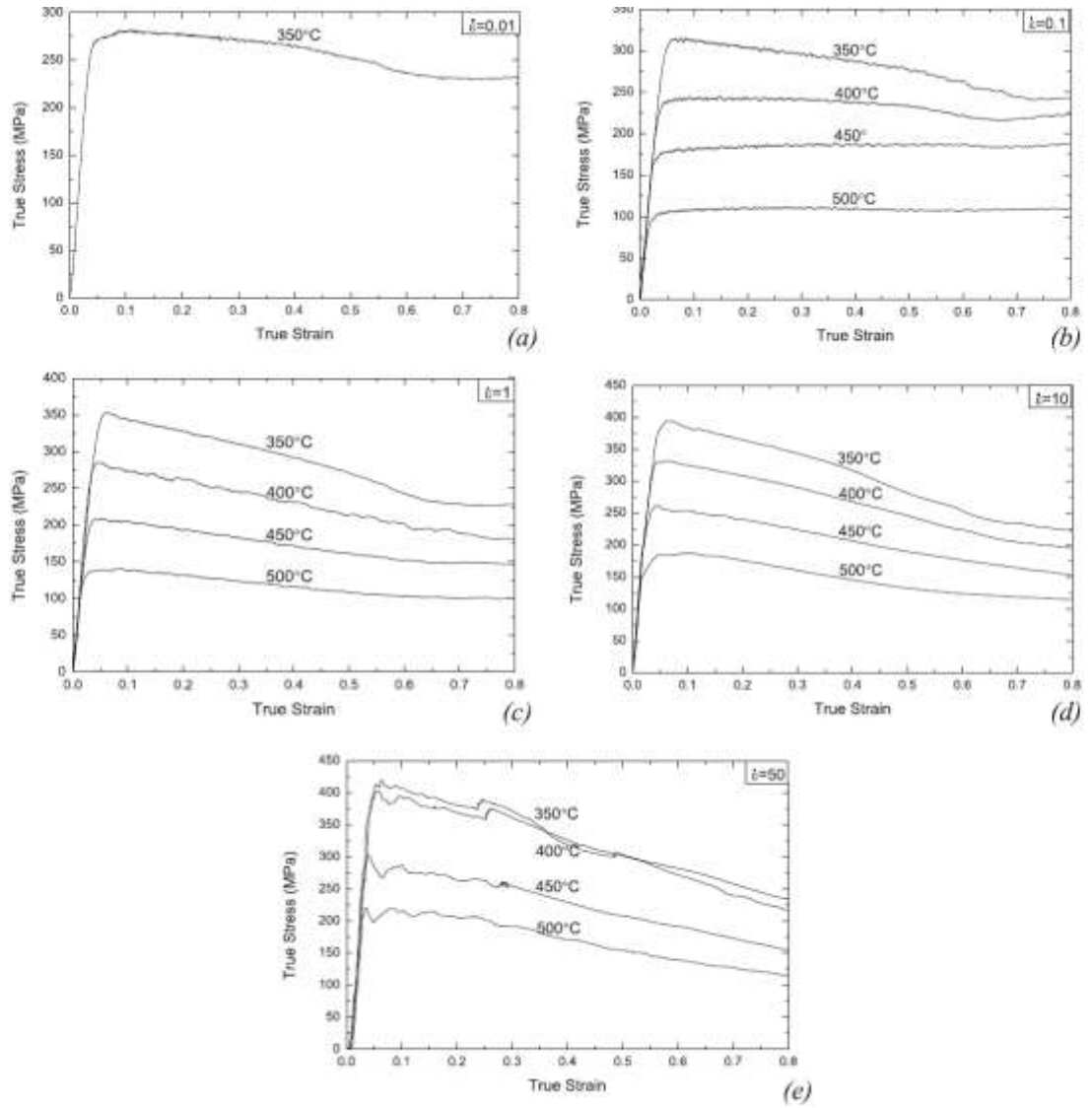


Fig. 5. Compression tests of the 10-1b bar at constant strain rate and varying temperature. (a) test performed at strain rate 0.01 s^{-1} and $T = 350 \text{ }^{\circ}\text{C}$. (b) tests performed at 0.1 s^{-1} and a varying temperature between $350\text{--}500 \text{ }^{\circ}\text{C}$, (c) tests performed at strain rate 1 s^{-1} and temperature between $350\text{--}500 \text{ }^{\circ}\text{C}$. (d) tests performed at strain rate 10 s^{-1} and temperature between $350\text{--}500 \text{ }^{\circ}\text{C}$, (e) tests performed at strain rate 50 s^{-1} and temperature between $350\text{--}500 \text{ }^{\circ}\text{C}$.

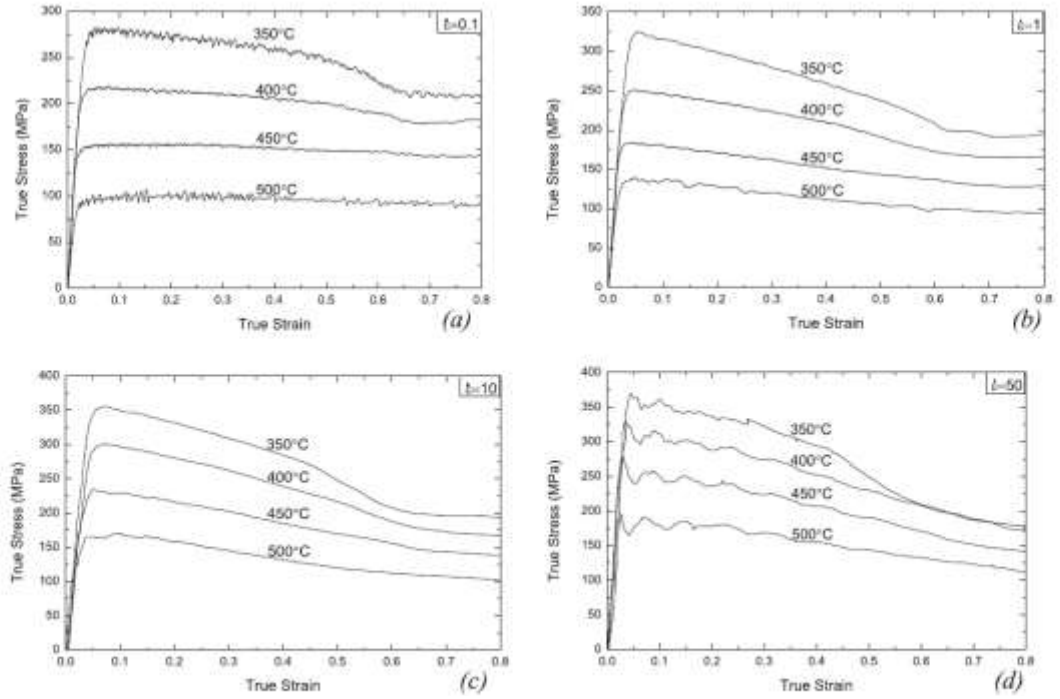


Fig. 6. Compression curves obtained by testing the 20-1b bar at constant strain rate and varying temperatures. (a) Tests at strain rate 0.1 s^{-1} and temperatures between 350–500 °C. (b) tests performed at strain rate 1 s^{-1} and temperatures 350–500 °C, (c) Tests performed at strain rate 10 s^{-1} and temperatures 350–500 °C. (d) tests performed at strain rate 50 s^{-1} and temperatures between 350–500 °C.

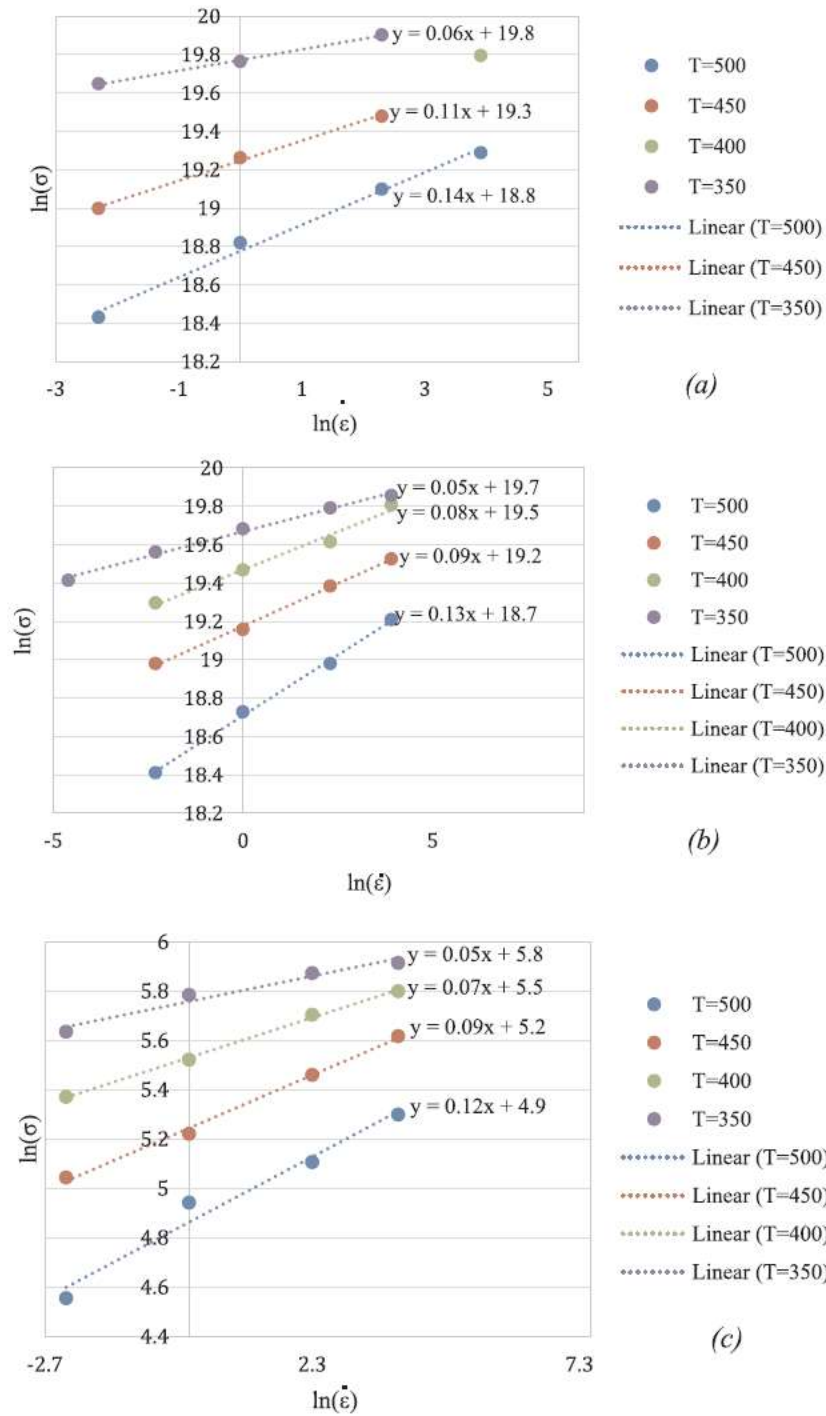


Fig. 7. The variation of $\ln(\text{steady state stress})$ with $\ln(\text{strain rate})$ at constant temperature of the bars (a) monolithic alloy bar, (b) +10 vol% fibres and (c) +20 vol% fibres used to determine the strain rate sensitivity parameter m .

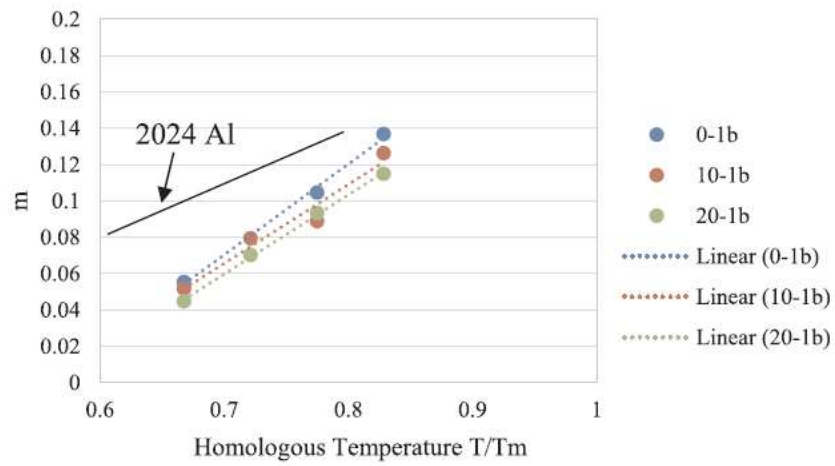


Fig. 8. Variation of strain rate sensitivity with temperature for the monolithic alloy bar, the one with 10 vol% fibres and the one with 20 vol% fibres, between 350 and 500 °C compared to the values for 2024 Al alloy [22].

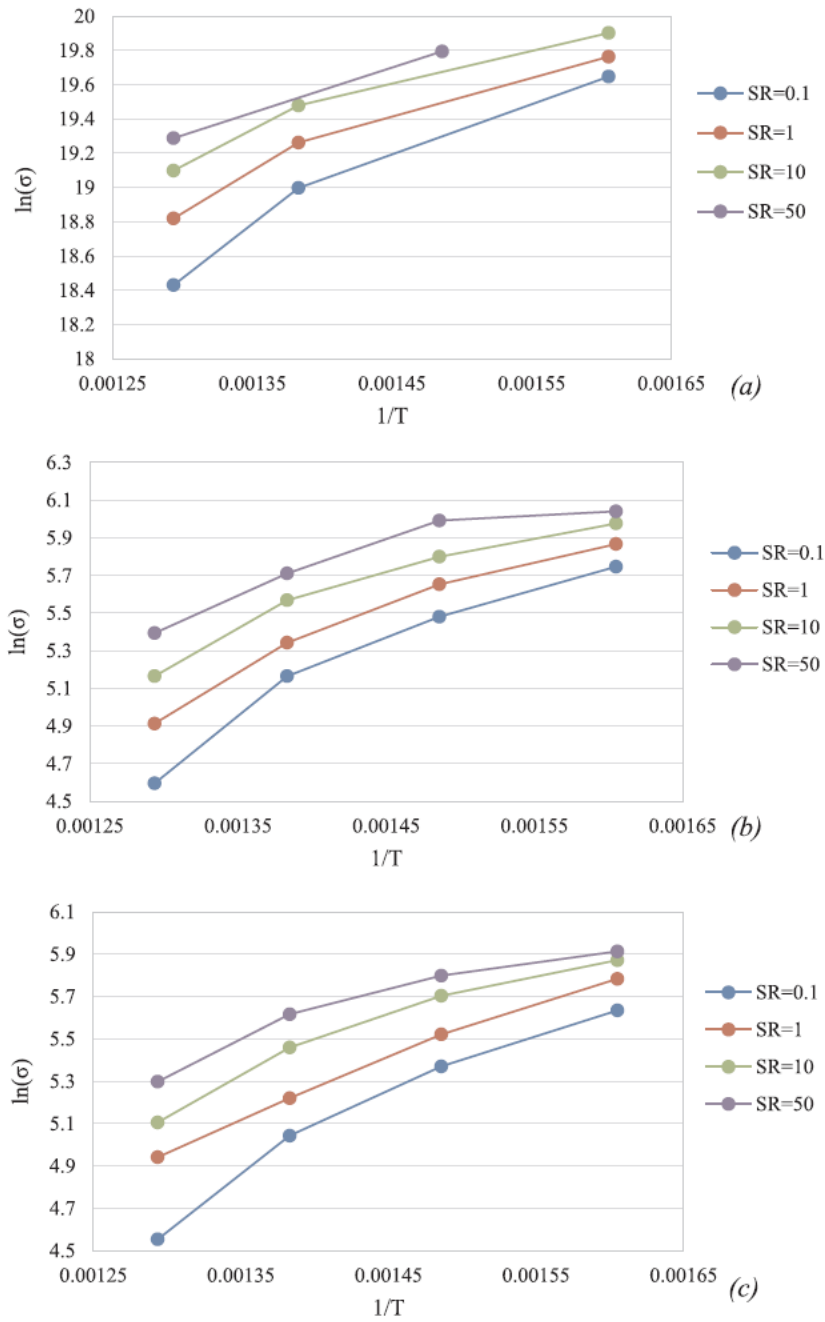


Fig. 9. Plot of $\ln(\sigma)$ and $1/T$ used at steady state to determine the apparent activation energy required of the microstructural mechanisms which govern the plastic flow behaviour of the material.

Tables

Table 1
elemental composition of the elongated, nodular Fe-enriched intermetallic phases measured by TEM-EDX.

Element	Intermetallic phases in Fig. 4 (b). at%	Error
Al	95.2	0.3
Ti	0.1	0.2
Cr	0.4	0.4
Fe	4.3	0.7

Table 2
Calculations of interaction energies and diffusion coefficients at the selected experimental setup.

Diffusing element	Fe	Cr	Ti
Tmin for each element/ K	~440 [12]	~413 [26]	~500–525 [12]
C0 in solid solution (at%)	0.2±0.1	0.4±0.2	1.3±0.2
Wmin (using Tmin from lit.)/ J/atom	-5.6×10^{-21}	-1.3×10^{-21}	6.6×10^{-21} (at 500 K)
			6.9×10^{-21} (at 525 K)
D using Tmin from lit./ m ² /s	7.3×10^{-17}	1.1×10^{-16}	4.3×10^{-18}
D at the testing temperature of 625 K/m ² /s	1.0×10^{-16}	1.6×10^{-16}	5.2×10^{-18}